LUND UNIVERSITY

A Fast and Stable Solver for Singular Integral Equations on Piecewise Smooth Curves

Helsing, Johan

Link to publication

Total number of authors:
1

LUND UNIVERSITY

PO Box 117
221 00 Lund
+46 46-222 00 00

A FAST AND STABLE SOLVER FOR SINGULAR INTEGRAL EQUATIONS ON PIECEWISE SMOOTH CURVES[*]

JOHAN HELSING[†]

Abstract. A scheme for the numerical solution of singular integral equations on piecewise smooth curves is presented. It relies on several techniques: reduction, Nyström discretization, composite quadrature, recursive compressed inverse preconditioning, and multipole acceleration. The scheme is fast and stable. Its computational cost grows roughly logarithmically with the precision sought and linearly with overall system size. When the integral equation models a boundary value problem, the achievable accuracy may be close to the condition number of that problem times machine epsilon. This is illustrated by application to elastostatic problems involving zigzag-shaped cracks with up to twenty thousand corners and branched cracks with hundreds of triple junctions.

Key words. singular integral equation, elasticity, corner singularity, multiwedge points

AMS subject classifications. 45E05, 65R20, 74B05

DOI. 10.1137/090779218

1. Introduction. Integral equation methods are comparatively popular for solving computational problems in fracture mechanics. A reason for this may be their ability to cheaply and accurately resolve the strong singularities that arise in stress fields close to endpoints such as crack tips and points on smooth outer boundaries or interfaces where the boundary conditions change type.

1.1. Singular integral equations. When modeling planar crack problems and, more generally, boundary value problems with mixed conditions on contiguous boundary parts [23], one often arrives at singular integral equations of the type

$$K\omega(z) + k\omega(z) = g(z), \quad z \in \Gamma,$$ (1.1)

where $\omega(z)$ is a layer density to be solved for, $g(z)$ is a piecewise smooth right-hand side, and K and k are integral operators

$$K\omega(z) = a(z)\omega(z) + \frac{b(z)}{\pi \mathrm{i}} \int_\Gamma \frac{\omega(\tau)\,\mathrm{d}\tau}{\tau - z},$$ (1.2)

$$k\omega(z) = \frac{1}{\pi \mathrm{i}} \int_\Gamma \omega(\tau) k(\tau, z)\,\mathrm{d}\tau.$$ (1.3)

Here τ and z are points in the complex plane, Γ is a curve, $a(z)$ and $b(z)$ are piecewise constant functions on Γ, and the kernel $k(\tau, z)$ is smooth wherever Γ is smooth so that k is a compact operator on a smooth Γ. The Cauchy singular integral in (1.2) is to be interpreted in the principal value sense. If $|b(z)| > |a(z)|$ on parts of Γ, and depending on in what function space $\omega(z)$ is sought, then the index of the dominant operator K may be nonzero, and additional constraints have to be added for uniqueness or solvability. See sections 79 and 109 in Muskhelishvili [25].

[†]Numerical Analysis, Centre for Mathematical Sciences, Lund University, Box 118, SE-221 00 Lund, Sweden (helsing@maths.lth.se).

1.2. General solution strategies. Singular integral equations of the type (1.1) may be solved numerically as they stand. Alternatively, they can be transformed into hypersingular equations or reduced to Fredholm second kind equations with compositions of integral operators and then solved numerically. See Chen [3] for a review. When the boundary parts are smooth and well separated, all three approaches can produce good results. Some simple geometries even allow for closed form solutions. Loosely speaking, this is because the (pseudo-) inverse K^+ (called regularizator in [24]) of K can be written in closed form, and the remaining compact operator is easy to deal with. The action of K^+ on a function $f(z)$ is

$$(1.4) \qquad K^+ f(z) = \frac{a(z)f(z)}{a^2(z) - b^2(z)} - \frac{b(z)\rho(z)}{(a^2(z) - b^2(z))} \frac{1}{\pi i} \int_\Gamma \frac{f(\tau)\,d\tau}{\rho(\tau)(\tau - z)},$$

where $\rho(z)$, called $Z(t)$ in [25, section 107], is a fundamental function which depends globally on the geometry. Although the precise choice of integral equation may not be important in all situations, it is the opinion of the present author that reduced second kind equation formulations are to be preferred, particularly so when $|b(z)| > |a(z)|$. Reduced formulations offer flexibility in terms of discretization and overall stability due to their spectral properties. High accuracy and computational speed can be obtained with coarse meshes, also for large-scale problems. The literature on integral equation methods for crack problems is rich; see the references in [3]. Further examples include [8, 18, 22, 30] on internal cracks, [17, 26] on interface cracks, [10] on edge cracks, and [5, 21] on contacting cracks.

1.3. Nonsmooth boundaries. In damage evolution, fractured specimens seldom have boundaries that are entirely smooth. Cracks may initiate at edges and notch tips, grow in zigzag-like patterns, and split up into branches [16, 27]. The appearance of *singular boundary points* such as corner vertices and triple junctions has consequences for numerics: The nature of the integral equations changes. The operator k in (1.1) is not compact at the singular points, and solutions exhibit complicated asymptotic behavior in their vicinity. Local mesh refinement is needed. Spectra of system matrices grow, and ill-conditioning is added. Iterative methods converge progressively slower. Eventually the accuracy suffers as well.

Figure 1.1, whose creation will be detailed in later sections, illustrates this phenomenon for the simple case of a V-shaped crack in an elastic plane under load. A reduced second kind equation is discretized with a Nyström method based on composite 16-point quadrature and solved iteratively. A quantity called the stress intensity factor is computed from the solution. A coarse mesh with eight quadrature panels on the crack face is used as a start. Then the panels closest to the singular boundary point are repeatedly subdivided. After n subdivisions there are $32(4 + n)$ unknowns. The left image of Figure 1.1 shows that beyond $n = 40$, the rounding error dominates the discretization error and further refinement is counterproductive. The right image shows how the number of iterations increase. Let E be the relative error sought in the solution. The computational work needed to achieve E grows roughly as $(\log(10^{-4}/E))^3$, provided that E is reached before the instability develops.

1.4. The need for better algorithms. Should one be worried about Figure 1.1? After all, we get four accurate digits already on the coarse mesh and ten digits at a cost of 1200 extra unknowns and twice the number of iterations. How high a precision does one really need? Judging from the literature, it seems as if improving the situation in Figure 1.1 is not a major issue. See, however, Englund [10] for a successful
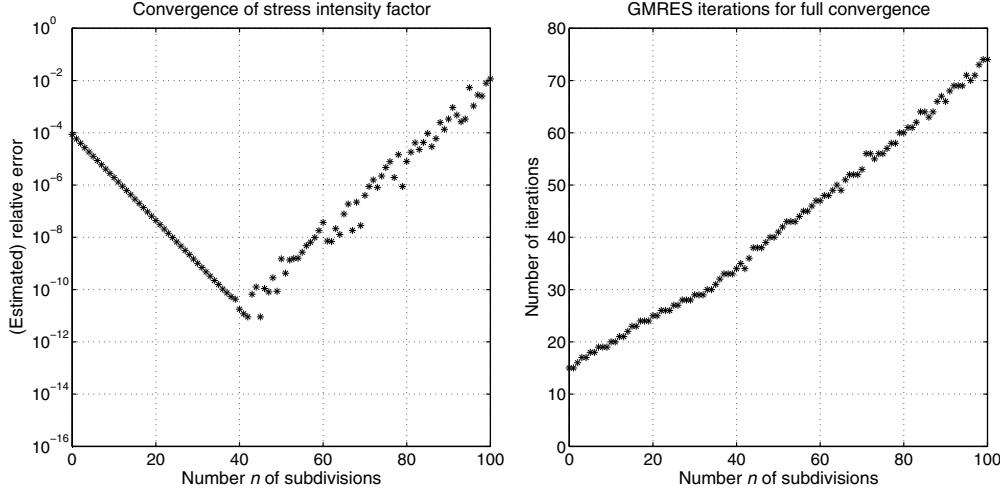
FIG. 1.1. *Convergence with mesh refinement for a reduced singular integral equation modeling a V-shaped crack under load. Left: Convergence of the stress intensity factor. Right: the number of* GMRES *iterations needed to reach a stopping criterion threshold of* ϵ_{mach} *in the relative residual.*

attempt at bringing down the number of iterations via numerical left preconditioning. As for better algorithms, we argue as follows: the V-shaped crack is very simple. There is nothing ill-conditioned whatsoever about the determination of its stress intensity factor under various loads. Therefore better algorithms must be possible. Moreover, in realistic large-scale damage evolution models, where stress fields are to be computed repeatedly for propagating and interacting cracks, speed and stability are crucial for efficiency. Unstable algorithms can exhibit seriously aggravated behavior compared to Figure 1.1. Tracing the path of just one crack accurately in a quasi-static crack growth simulation is, for a mix of reasons, a formidable challenge. See [11, 27] for the state of the art in this field. Therefore, better algorithms are needed.

1.5. Particular difficulties. Reduction of (1.1) via application of K^+ from the left gives

$$(1.5) \qquad \omega(z) + K^+ k \omega(z) = K^+ g(z), \quad z \in \Gamma.$$

In order to solve this reduced equation efficiently on piecewise smooth curves, and in view of the discussion in section 1.3, some nonstandard quadrature technique— perhaps a set of special quadrature weights—is needed for the action of k on $\omega(z)$ close to singular boundary points. Not only that, yet another application of nonstandard quadrature is needed for the action of K^+ on $k\omega(z)$.

There are several difficulties here: the asymptotic behavior of $\omega(z)$ and $k\omega(z)$ may differ, K^+ is a Cauchy singular operator, and the right-hand side of (1.5) is not smooth. This is a much more involved situation than that covered by the recent techniques for nonsingular integral equations, free from composed integral operators, on piecewise smooth curves [1, 20]. Furthermore, K^+ depends globally on the geometry via the fundamental function. This function appears both in the integrand, $\rho(\tau)$, and outside of it, $\rho(z)$; see (1.4). The quadrature for K^+ either has to be insensitive to the fine details of K^+, or a new quadrature has to be constructed whenever the geometry changes. In the simulation of a growing crack the global geometry changes at each simulation step, making this a crucial point for computational efficiency.

1.6. New development. The purpose of this paper is to construct a fast and stable algorithm for singular integral equations of the type (1.1) with $|b(z)| > |a(z)|$ on piecewise smooth curves with many singular boundary points. We shall work with reduced second kind formulations and composed integral operators.

Our strategy is to extend the applicability of the method dubbed *recursive compressed inverse preconditioning* in [20]. Conceptually this is a local multilevel technique which makes a change of basis and expresses the nonsmooth original layer density in terms of a piecewise smooth transformed layer density which can be cheaply resolved by polynomials. Discretization leads to a block diagonal transformation matrix $\mathbf{R}$ (a right inverse preconditioner), where the columns of a particular block can be interpreted as special basis functions for the original density in the vicinity of a singular boundary point multiplied with suitable quadrature weights. The blocks of $\mathbf{R}$ are constructed in a fast recursion, $i = 1, \ldots, n$, where step i inverts and compresses contributions to $\mathbf{R}$ involving the outermost quadrature panels on level i of a locally n-ply refined mesh.

The need for different quadratures for different operators will, in the present paper, be met by introducing four matrices $\mathbf{R}_m$, which are related to each other blockwise and constructed simultaneously. The global dependence on the geometry in K^+ will be factored out from the recursion, making the blocks of the $\mathbf{R}_m$ matrices strictly local quantities which can be reused as a geometry evolves.

Let c_0 be the cost of solving a reduced singular integral equation with a standard method on a coarse mesh, sufficiently refined as to resolve the problem away from the singular boundary points. Let E_0 be the precision of the corresponding solution. The computational cost of achieving a relative error E with our scheme will be roughly $c_0 + O(\log(E_0/E))$.

1.7. Organization of the paper. Section 2 contains definitions. Some restrictions are made to prevent the paper from becoming too lengthy. Section 3 introduces inverse preconditioning and rewrites (1.1) so that the unknown layer density becomes piecewise smooth. Section 4 focuses on discretization and compression. A coarse mesh will be sufficient for high resolution provided that the transformation matrices $\mathbf{R}_m$ are available. Their rapid construction is the topic of section 5. Application to crack problems is discussed in section 6. Numerical examples are given in section 7.

2. Preliminaries. This section defines various concepts and constructions that will be used throughout the paper.

2.1. The dominant operator. For brevity we specialize to the case $a(z) = 0$ and $b(z) = 1$ in K of (1.2). This case seems to arise frequently in fracture mechanics.

2.2. The curve. Let Γ be a connected curve in an infinite plane which is a union of a number of oriented smooth open arcs such that Γ has p endpoints, $p-2$ branching points where three arcs meet, and q corner points where two arcs meet. The endpoints are denoted γ_i^{ep}, $i = 1, \ldots, p$. The branching points are denoted γ_j^{bp}, $j = 1, \ldots, p-2$. The corner points are denoted γ_l^{cp}, $l = 1, \ldots, q$. The outward unit normal of Γ at z is denoted n_z. The plane outside of Γ is denoted D. For simplicity we assume that γ_i^{ep}, γ_j^{bp}, and γ_l^{cp} are not located too close to each other. See Figure 2.1 for two examples.

2.3. Meshes. We shall construct two different meshes on Γ for the purpose of discretization. Let Γ first be divided into coarse panels of approximately equal length and such that no coarse panel has a branching point or a corner point as an interior point. This is the *coarse mesh*. Let $\Gamma_j^{\star\mathrm{bp}}$ be the segment of Γ covering the six coarse
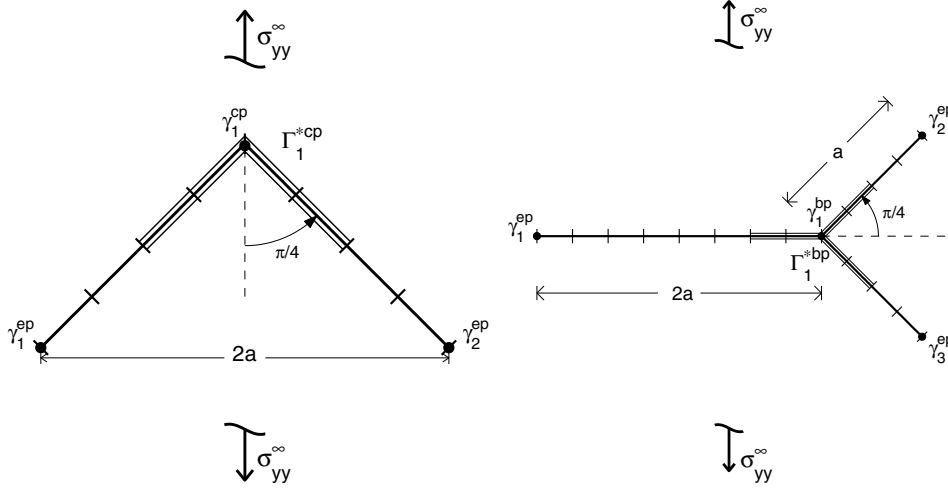
FIG. 2.1. *Left:* Γ *has* $p = 2$ *endpoints and* $q = 1$ *corner point. Right:* Γ *has* $p = 3$ *endpoints and* $p - 2 = 1$ *branching point. A coarse mesh is constructed on both curves. The four coarse panels closest to* γ_1^{cp} *form* $\Gamma_1^{\star\mathrm{cp}}$. *The six coarse panels closest to* γ_1^{bp} *form* $\Gamma_1^{\star\mathrm{bp}}$. *These segments are indicated with extra double lines. When used in numerical examples, the curves are called the "V-shaped crack" and the "symmetrically branched crack," and a uniaxial load is applied at infinity.*

panels closest to γ_j^{bp} and let $\Gamma_l^{\star\mathrm{cp}}$ be the segment of Γ covering the four coarse panels closest to γ_l^{cp}; see Figure 2.1. Let $\Gamma^\star$ be the union of all $p + q - 2$ (nonoverlapping) such curve segments. Now, let the innermost coarse panels on each $\Gamma_j^{\star\mathrm{bp}}$ and $\Gamma_l^{\star\mathrm{cp}}$ be n times subdivided in a direction toward γ_j^{bp} or γ_l^{cp}. This is the *fine mesh*, and we say that it is n-ply refined relative to the coarse mesh.

2.4. The fundamental function. With $a(z) = 0$ and $b(z) = 1$ in (1.2), one can choose the fundamental function $\rho(z)$ as

$$(2.1) \qquad \rho(z) = \prod_{i=1}^{p}(z - \gamma_i^{\mathrm{ep}})^{-1/2} \prod_{j=1}^{p-2}(z - \gamma_j^{\mathrm{bp}})^{1/2}, \quad z \in D,$$

corresponding to seeking $\omega(z)$ in a class of solutions to (1.1) with index one; see section 107 of [25]. The value of $\rho(z)$ for $z \in \Gamma$ is defined as the limit from the right of the branch given by a cut along Γ and $z\rho(z) = 1$ at infinity.

The evaluation of $\rho(z)$ is described in detail in section 4 of [9], and we shall follow that procedure. In addition, we allow for a factorization

$$(2.2) \qquad \rho(z) = \rho_{\mathrm{G}}(z)\rho_{\mathrm{L}}(z),$$

where the *local factor* $\rho_{\mathrm{L}}(z)$ captures the part of $\rho(z)$ that varies rapidly close to the branching points. That is, $\rho_{\mathrm{L}}(z) = (z - \gamma_j^{\mathrm{bp}})^{1/2}$ on $\Gamma_j^{\star\mathrm{bp}}$ and unity otherwise. The *global factor* $\rho_{\mathrm{G}}(z)$ will be piecewise smooth away from the endpoints γ_i^{ep}.

The choice of $\rho(z)$ in (2.1) makes the index of the Fredholm operator $K\rho$ (between some weighted L^2 spaces) equal to one, and

$$(2.3) \qquad K\rho K\rho^{-1} = I$$

holds so that $\rho K\rho^{-1}$ is a right inverse to K.

2.5. The reduced equation. The behavior of $\omega(z)$ at the endpoints of Γ is similar to that of the fundamental function. This follows from the form of K^+ in (1.4). For numerical reasons it is beneficial to factor out $\rho(z)$ from $\omega(z)$,

$$(2.4) \qquad\qquad\qquad \omega(z) = \rho(z)\omega_0(z) \,,$$

so that the new unknown $\omega_0(z)$ varies less. Equation (1.1) then reads

$$(2.5) \qquad\qquad K\rho\omega_0(z) + k\rho\omega_0(z) = g(z) \,, \quad z \in \Gamma \,.$$

This equation has a nontrivial homogeneous solution. For uniqueness we add the constraint

$$(2.6) \qquad\qquad\qquad \int_\Gamma \rho(\tau)\omega_0(\tau)\,\mathrm{d}\tau = 0 \,,$$

which is common in fracture mechanics. Equation (2.5) can be reduced to

$$(2.7) \qquad\qquad \Omega(z) + k\rho K\rho^{-1}\Omega(z) = g(z) \,, \quad z \in \Gamma \,,$$

using (2.3) and the substitution

$$(2.8) \qquad\qquad\qquad \omega_0(z) = K\rho^{-1}\Omega(z),$$

which makes $\omega_0(z)$ satisfy (2.6).

3. Inverse preconditioning. This section shows how to rewrite the reduced equation (2.7) so that the unknown layer density becomes piecewise smooth.

3.1. A split equation. Let k of (1.1) be split into two operators

$$(3.1) \qquad\qquad\qquad k = k^\star + k^\circ \,.$$

Here $k^\star$ is equal to k when z and τ simultaneously lie on the same curve segment $\Gamma_j^{\star\mathrm{bp}}$ or $\Gamma_l^{\star\mathrm{cp}}$, and zero otherwise. The operator k° is compact. We say that $k^\star$ describes *self-interaction* of k on $\Gamma^\star$.

Let K and I be split according to the same pattern

$$(3.2) \qquad\qquad K = K^\star + K^\circ \,, \quad I = I^\star + I^\circ \,.$$

Furthermore, let the operator $K^\sharp$ be defined by the split

$$(3.3) \qquad\qquad K = \rho_\mathrm{G}^{-1}K^\star\rho_\mathrm{G} + K^\sharp \,,$$

so that

$$(3.4) \qquad\qquad K^\sharp = K^\circ + (K^\star - \rho_\mathrm{G}^{-1}K^\star\rho_\mathrm{G}) \,.$$

The part of $K^\sharp$ which accounts for self-interaction on $\Gamma^\star$ (the term within parentheses in (3.4)) has a continuous kernel. Its action on a function produces smooth output on $\Gamma^\star$. The other part, K°, produces smooth output on the innermost coarse panels of each $\Gamma_j^{\star\mathrm{bp}}$ and $\Gamma_l^{\star\mathrm{cp}}$.

In terms of the split matrices of (3.1) and (3.3), one can rewrite (2.7) as

$$(3.5) \quad \left(I + k^\star\rho_\mathrm{L}K^\star\rho_\mathrm{L}^{-1} + k^\circ\rho K^\sharp\rho^{-1} + k^\circ\rho_\mathrm{L}K^\star\rho_\mathrm{L}^{-1} + k^\star\rho K^\sharp\rho^{-1}\right)\Omega(z) = g(z) \,.$$

3.2. Smooth unknowns. Using the substitution

$$(3.6) \qquad \Omega(z) = R\left(\tilde{\Omega}_1(z) + k^\star \rho_{\mathrm{L}} \tilde{\Omega}_2(z)\right),$$

where the right inverse preconditioner R is

$$(3.7) \qquad R = \left(I + k^\star \rho_{\mathrm{L}} K^\star \rho_{\mathrm{L}}^{-1}\right)^{-1},$$

and where the layer density $\tilde{\Omega}_2(z)$ only has support on $\Gamma^\star$, one arrives at the right preconditioned equation

$$(3.8) \quad \left(I + (k^\circ \rho K^\sharp \rho^{-1} + k^\circ \rho_{\mathrm{L}} K^\star \rho_{\mathrm{L}}^{-1} + k^\star \rho K^\sharp \rho^{-1})R\right)\left(\tilde{\Omega}_1(z) + k^\star \rho_{\mathrm{L}} \tilde{\Omega}_2(z)\right) = g(z).$$

An interesting aspect of (3.8) is that the operator k° produces piecewise smooth output when it acts on a function, while $k^\star$ does not. Therefore, assuming that $g(z)$ is piecewise smooth, all nonsmooth terms on the left-hand side must sum up to zero, and we can expand (3.8) into a coupled system of two integral equations for the two transformed layer densities $\tilde{\Omega}_1(z)$ and $\tilde{\Omega}_2(z)$:

$$(3.9) \qquad \tilde{\Omega}_1(z) + (k^\circ \rho K^\sharp \rho^{-1} + k^\circ \rho_{\mathrm{L}} K^\star \rho_{\mathrm{L}}^{-1})R\left(\tilde{\Omega}_1(z) + k^\star \rho_{\mathrm{L}} \tilde{\Omega}_2(z)\right) = g(z),$$

$$(3.10) \qquad \tilde{\Omega}_2(z) + \rho_{\mathrm{G}} K^\sharp \rho^{-1} R\left(\tilde{\Omega}_1(z) + k^\star \rho_{\mathrm{L}} \tilde{\Omega}_2(z)\right) = 0.$$

The preconditioned system (3.9), (3.10) can be viewed as a variant of (2.7) that is potentially better suited for numerics. The density $\tilde{\Omega}_1(z)$ is piecewise smooth on Γ thanks to k° in (3.9). The density $\tilde{\Omega}_2(z)$ is piecewise smooth on the innermost coarse panels of each $\Gamma_j^{\star\mathrm{bp}}$ and $\Gamma_l^{\star\mathrm{cp}}$ thanks to $K^\sharp$ in (3.10); see the discussion following (3.4). Smooth unknowns are easy to resolve. Note, however, that some of the operators in (3.9), (3.10) may be difficult to resolve. When discretized on the same grid, solutions to (2.7) and to (3.9), (3.10) with (3.6) have the same discretization error.

4. Compressed discretization. This section focuses on discretization. In particular, we shall discretize the system (3.9), (3.10) on a grid on a fine mesh and compress the resulting discretization onto a grid on a coarse mesh without loss of precision. A new discrete layer density further cuts down the number of unknowns.

4.1. Quadrature techniques. Let $\tau(t)$ be a parameterization of Γ. We discretize (2.7) and (3.9), (3.10) using Nyström discretization and composite quadrature in t. On each quadrature panel, nodes t_j are placed according to 16-point Gauss–Legendre quadrature for a total of N nodes. The corresponding discretization points are denoted $\tau_j = \tau(t_j)$. In general, we choose quadrature weights according to Gauss–Legendre quadrature which is of polynomial degree 31. For τ on panels neighboring endpoints and branching points, we use quadrature weights constructed via product integration which are suitable for integration of functions $f(s) = f_0(s)/\sqrt{s}$ or $f(s) = f_0(s)\sqrt{s}$, where $f_0(s)$ is smooth and s is the distance to the endpoint or the branching point. These weights give polynomial degree 15. The collections of quadrature weights along Γ are denoted w_{1i} or w_{2i} depending on whether they are intended for integration of smooth functions $f_0(z)$ multiplied with ρ^{-1} or with ρ and will be referred to as our basic quadrature. Note that $\rho(z)$ and $\rho_{\mathrm{L}}(z)$ have the same asymptotics close to branching points. The same quadrature weights can be used for both functions.

4.2. The discretization of $K\rho^{-1}$. The action of the operator $K\rho^{-1}$ on a function $f(z)$ can be evaluated numerically in many ways. For example, one can use the *global regularization* formula

$$(4.1) \qquad K\rho^{-1}f(z) = \frac{1}{\pi\mathrm{i}} \int_\Gamma \frac{(f(\tau) - f(z))\,\mathrm{d}\tau}{\rho(\tau)(\tau - z)} + f(z)\left(z - \sum_{i=1}^{p} \frac{\gamma_i^{\mathrm{ep}}}{2} + \sum_{j=1}^{p-2} \frac{\gamma_j^{\mathrm{bp}}}{2} \right),$$

which can be discretized within a Nyström scheme using basic quadrature and differentiation of $f(\tau)$ based on panelwise polynomial interpolation at the nodes. We use this when $z \notin \Gamma^\star$, that is, only in connection with $K^\sharp \rho^{-1}$.

Drawbacks with global regularization include the following: it involves a fair amount of row summation for the diagonal elements of the system matrix; it performs poorly when $f(\tau)$ is discontinuous at the end of the panel on which a discretization point τ_j is situated; and it couples the quadrature on consecutive panels in a way that makes it hard to split up the integral into independent parts. A better alternative, in these respects, is *local panelwise evaluation*. Let τ_j be situated on a panel $\Lambda_2^\star$. Let $\Lambda_1^\star$ and $\Lambda_3^\star$ be the panels neighboring $\Lambda_2^\star$. Let $\Gamma_{123}^\star$ be the union of these three panels. Define $\Gamma_{123}^\circ = \Gamma \setminus \Gamma_{123}^\star$. Then

$$(4.2) \qquad K\rho^{-1}(\tau_j) = \frac{1}{\pi\mathrm{i}} \int_{\Gamma_{123}^\circ} \frac{f(\tau)\,\mathrm{d}\tau}{\rho(\tau)(\tau - \tau_j)} + \sum_{l=1}^{3} \frac{1}{\pi\mathrm{i}} \int_{\Lambda_l^\star} \frac{f(\tau)\,\mathrm{d}\tau}{\rho(\tau)(\tau - \tau_j)}, \quad \tau_j \in \Lambda_2^\star,$$

should be efficient. The first integral can be discretized using basic quadrature with weights w_{1i}. The integrals in the sum can be computed individually via product integration. We shall use a modification of a fast 15th-degree accurate method, outlined in [19, section 5.3], and apply it when $z \in \Gamma^\star$, that is, in connection both with $K^\sharp \rho^{-1}$ and $K^\star \rho_{\mathrm{L}}^{-1}$. For panels $\Lambda_2^\star$ neighboring a branching point, one needs to add a fourth panel to $\Gamma_{123}^\star$.

The part of $K^\sharp$ which accounts for self-interaction on $\Gamma^\star$ has a continuous kernel and can be discretized with basic quadrature. The limit value for $\tau = z \in \Gamma^\star$ is computed via numerical differentiation of $\rho_{\mathrm{G}}(z)$.

4.3. Discretization on two meshes. We work with two discretizations and let boldface denote discretized quantities. One discretization is on a grid on the coarse mesh, and the other is on a grid on the fine mesh. We shall distinguish between the discretizations with subscripts "C" for coarse and "F" for fine. Integral operators now become full matrices or block diagonal matrices, for example, $\mathbf{K}^\sharp$ and $\mathbf{k}^\star$. Fundamental functions and the identity operator become diagonal matrices $\boldsymbol{\rho}$ and $\mathbf{I}$. Layer densities and the right-hand side become column vectors. With this notation, discretization of (2.7) on the two meshes reads as

$$(4.3) \qquad\qquad \left(\mathbf{I}_{\mathrm{C}} + \mathbf{k}_{\mathrm{C}} \boldsymbol{\rho}_{\mathrm{C}} \mathbf{K}_{\mathrm{C}} \boldsymbol{\rho}_{\mathrm{C}}^{-1} \right) \boldsymbol{\Omega}_{\mathrm{C}} = \mathbf{g}_{\mathrm{C}},$$

$$(4.4) \qquad\qquad \left(\mathbf{I}_{\mathrm{F}} + \mathbf{k}_{\mathrm{F}} \boldsymbol{\rho}_{\mathrm{F}} \mathbf{K}_{\mathrm{F}} \boldsymbol{\rho}_{\mathrm{F}}^{-1} \right) \boldsymbol{\Omega}_{\mathrm{F}} = \mathbf{g}_{\mathrm{F}}.$$

The linear system (4.3) is $N_{\mathrm{C}} \times N_{\mathrm{C}}$, and the linear system (4.4) is $N_{\mathrm{F}} \times N_{\mathrm{F}}$.

We also need diagonal matrices whose nonzero elements are ratios between quadrature weights and corresponding pointwise values of fundamental functions. For this, define the square matrices $\mathbf{W}_1$ and $\mathbf{W}_2$ with nonzero entries

$$(4.5) \qquad W_{1jj} = \frac{w_{1j}}{\rho_{\mathrm{L}}(\tau_j)} \quad \text{and} \quad W_{2jj} = w_{2j}\rho_{\mathrm{L}}(\tau_j), \quad j = 1, \dots, N.$$

Let $\mathbf{P}_0$ be a discrete prolongation operator that performs panelwise 15th-degree polynomial interpolation in parameter from the coarse grid to the fine grid. Let $\mathbf{P}_1$ and $\mathbf{P}_2$ be weighted prolongation operators

$$(4.6) \qquad \mathbf{P}_l = \mathbf{W}_{l\mathrm{F}}\mathbf{P}_0\mathbf{W}_{l\mathrm{C}}^{-1}, \quad l = 1, 2 .$$

The prolongation operators have interesting properties. For example, one can show that the block diagonal matrices $\mathbf{P}_1^T\mathbf{P}_0$ and $\mathbf{P}_2^T\mathbf{P}_0$, where superscript T denotes the transpose, are the identity except on coarse panels neighboring branching points. It holds, however, also on such panels that

$$(4.7) \qquad \mathbf{f}_{i\mathrm{C}}^T\mathbf{W}_{l\mathrm{C}}\mathbf{P}_l^T\mathbf{P}_0\mathbf{f}_{j\mathrm{C}} = \mathbf{f}_{i\mathrm{C}}^T\mathbf{W}_{l\mathrm{C}}\mathbf{f}_{j\mathrm{C}}, \quad l = 1, 2 ,$$

where $\mathbf{f}_{i\mathrm{C}}$ and $\mathbf{f}_{j\mathrm{C}}$ are discretizations of piecewise polynomials on the coarse grid of degree i and j, whenever $i + j \leq 15$. While $\mathbf{P}_l^T\mathbf{P}_0$ certainly is computable, in view of (4.7), we shall use the approximations

$$(4.8) \qquad \mathbf{P}_l^T\mathbf{P}_0 = \mathbf{I}, \quad l = 1, 2 ,$$

which then hold either exactly or to the same polynomial degree as product integration and local panelwise evaluation.

4.4. Compression. We discretize (3.9), (3.10) on the fine grid. Under the assumption that the coarse mesh is sufficiently resolved for

$$(4.9) \qquad \mathbf{k}_{\mathrm{F}}^{\circ}\boldsymbol{\rho}_{\mathrm{F}} = \mathbf{P}_0\mathbf{k}_{\mathrm{C}}^{\circ}\boldsymbol{\rho}_{\mathrm{C}}\mathbf{P}_2^T ,$$

$$(4.10) \qquad \mathbf{K}_{\mathrm{F}}^{\sharp}\boldsymbol{\rho}_{\mathrm{F}}^{-1} = \mathbf{P}_0\mathbf{K}_{\mathrm{C}}^{\sharp}\boldsymbol{\rho}_{\mathrm{C}}^{-1}\mathbf{P}_1^T ,$$

$$(4.11) \qquad \mathbf{g}_{\mathrm{F}} = \mathbf{P}_0\mathbf{g}_{\mathrm{C}} ,$$

to hold accurately, the system (3.9), (3.10) on the fine grid can be compressed onto the coarse grid without loss of precision (discretization error). The compression procedure relies on substituting (4.9)–(4.11) into the discretized system (3.9), (3.10) and on using (4.8) and, implicitly, the smoothness of $\tilde{\Omega}_1(z)$ and $\tilde{\Omega}_2(z)$. Full details, in an analogous situation, are given in [20, section 6.4]. The compressed equations corresponding to (3.9), (3.10) read as

$$(4.12) \quad \tilde{\boldsymbol{\Omega}}_{1\mathrm{C}} + \mathbf{k}_{\mathrm{C}}^{\circ}\boldsymbol{\rho}_{\mathrm{C}}\mathbf{K}_{\mathrm{C}}^{\sharp}\boldsymbol{\rho}_{\mathrm{C}}^{-1}\left(\mathbf{R}_1\tilde{\boldsymbol{\Omega}}_{1\mathrm{C}} + \mathbf{R}_3\tilde{\boldsymbol{\Omega}}_{2\mathrm{C}}\right) + \mathbf{k}_{\mathrm{C}}^{\circ}\boldsymbol{\rho}_{\mathrm{LC}}\left(\mathbf{R}_2\tilde{\boldsymbol{\Omega}}_{1\mathrm{C}} + \mathbf{R}_4\tilde{\boldsymbol{\Omega}}_{2\mathrm{C}}\right) = \mathbf{g}_{\mathrm{C}} ,$$

$$(4.13) \quad \tilde{\boldsymbol{\Omega}}_{2\mathrm{C}} + \mathbf{I}_{\mathrm{C}}^{\star}\boldsymbol{\rho}_{\mathrm{GC}}\mathbf{K}_{\mathrm{C}}^{\sharp}\boldsymbol{\rho}_{\mathrm{C}}^{-1}\left(\mathbf{R}_1\tilde{\boldsymbol{\Omega}}_{1\mathrm{C}} + \mathbf{R}_3\tilde{\boldsymbol{\Omega}}_{2\mathrm{C}}\right) = \mathbf{0} ,$$

where only the compressed weighted inverses

$$(4.14) \qquad \mathbf{R}_1 = \mathbf{P}_1^T\left(\mathbf{I}_{\mathrm{F}}^{\star} + \mathbf{k}_{\mathrm{F}}^{\star}\boldsymbol{\rho}_{\mathrm{LF}}\mathbf{K}_{\mathrm{F}}^{\star}\boldsymbol{\rho}_{\mathrm{LF}}^{-1}\right)^{-1}\mathbf{P}_0 + \mathbf{I}_{\mathrm{C}}^{\circ} ,$$

$$(4.15) \qquad \mathbf{R}_2 = \mathbf{P}_2^T\mathbf{K}_{\mathrm{F}}^{\star}\boldsymbol{\rho}_{\mathrm{LF}}^{-1}\left(\mathbf{I}_{\mathrm{F}}^{\star} + \mathbf{k}_{\mathrm{F}}^{\star}\boldsymbol{\rho}_{\mathrm{LF}}\mathbf{K}_{\mathrm{F}}^{\star}\boldsymbol{\rho}_{\mathrm{LF}}^{-1}\right)^{-1}\mathbf{P}_0 ,$$

$$(4.16) \qquad \mathbf{R}_3 = \mathbf{P}_1^T\left(\mathbf{I}_{\mathrm{F}}^{\star} + \mathbf{k}_{\mathrm{F}}^{\star}\boldsymbol{\rho}_{\mathrm{LF}}\mathbf{K}_{\mathrm{F}}^{\star}\boldsymbol{\rho}_{\mathrm{LF}}^{-1}\right)^{-1}\mathbf{k}_{\mathrm{F}}^{\star}\boldsymbol{\rho}_{\mathrm{LF}}\mathbf{P}_0 ,$$

$$(4.17) \qquad \mathbf{R}_4 = \mathbf{P}_2^T\mathbf{K}_{\mathrm{F}}^{\star}\boldsymbol{\rho}_{\mathrm{LF}}^{-1}\left(\mathbf{I}_{\mathrm{F}}^{\star} + \mathbf{k}_{\mathrm{F}}^{\star}\boldsymbol{\rho}_{\mathrm{LF}}\mathbf{K}_{\mathrm{F}}^{\star}\boldsymbol{\rho}_{\mathrm{LF}}^{-1}\right)^{-1}\mathbf{k}_{\mathrm{F}}^{\star}\boldsymbol{\rho}_{\mathrm{LF}}\mathbf{P}_0$$

need the fine grid for their construction.

Note that (4.14)–(4.17) are local quantities, that is, they do not depend on $\rho_{\mathrm{G}}(z)$. Furthermore, $\mathbf{R}_1$-$\mathbf{I}_{\mathrm{C}}^{\circ}$, $\mathbf{R}_2$, $\mathbf{R}_3$, and $\mathbf{R}_4$ have the same sparse block diagonal structure as $\mathbf{k}_{\mathrm{C}}^{\star}$. The matrix blocks associated with curve segments $\Gamma_j^{\star\mathrm{bp}}$ have size 96×96. The matrix blocks associated with curve segments $\Gamma_l^{\star\mathrm{cp}}$ have size 64×64.

4.5. A single equation. With the substitution

$$(4.18) \qquad \tilde{\boldsymbol{\Omega}}_{1C} = \hat{\boldsymbol{\Omega}}_C + \mathbf{R}_1^{-1}\mathbf{R}_3\boldsymbol{\rho}_{GC}\mathbf{K}_C^\sharp\boldsymbol{\rho}_C^{-1}\mathbf{R}_1\hat{\boldsymbol{\Omega}}_C\,,$$

$$(4.19) \qquad \tilde{\boldsymbol{\Omega}}_{2C} = -\mathbf{I}_C^\star\boldsymbol{\rho}_{GC}\mathbf{K}_C^\sharp\boldsymbol{\rho}_C^{-1}\mathbf{R}_1\hat{\boldsymbol{\Omega}}_C\,,$$

the combined system (4.12), (4.13) can be consolidated into the single system

$$\left(\mathbf{I}_C + \mathbf{k}_C^\circ\boldsymbol{\rho}_{LC}\left(\mathbf{I}_C + \mathbf{R}_2\mathbf{R}_1^{-1}\mathbf{R}_3 - \mathbf{R}_4\right)\boldsymbol{\rho}_{GC}\mathbf{K}_C^\sharp\boldsymbol{\rho}_C^{-1}\mathbf{R}_1\right.$$

$$(4.20) \qquad \left. + \mathbf{k}_C^\circ\boldsymbol{\rho}_{LC}\mathbf{R}_2 + \mathbf{R}_1^{-1}\mathbf{R}_3\boldsymbol{\rho}_{GC}\mathbf{K}_C^\sharp\boldsymbol{\rho}_C^{-1}\mathbf{R}_1\right)\hat{\boldsymbol{\Omega}}_C = \mathbf{g}_C\,,$$

reminiscent of a discretization of (3.8) on the coarse mesh. Once this $N_C \times N_C$ linear system is solved for $\hat{\boldsymbol{\Omega}}_C$, discrete values for the original density $\omega_0(z)$ can be obtained via (4.18), (4.19) and a discretization of (2.8) with (3.6), which reads as

$$(4.21) \qquad \boldsymbol{\omega}_{0C} = \mathbf{K}_C^\sharp\boldsymbol{\rho}_C^{-1}\mathbf{R}_1\hat{\boldsymbol{\Omega}}_C + \mathbf{I}_C^\star\boldsymbol{\rho}_{GC}^{-1}\left(\mathbf{S}_2\tilde{\boldsymbol{\Omega}}_{1C} + \mathbf{S}_4\tilde{\boldsymbol{\Omega}}_{2C}\right)\,,$$

where the compressed unweighted inverses

$$(4.22) \qquad \mathbf{S}_2 = \mathbf{Q}_0\mathbf{K}_F^\star\boldsymbol{\rho}_{LF}^{-1}\left(\mathbf{I}_F + \mathbf{k}_F^\star\boldsymbol{\rho}_{LF}\mathbf{K}_F^\star\boldsymbol{\rho}_{LF}^{-1}\right)^{-1}\mathbf{P}_0\,,$$

$$(4.23) \qquad \mathbf{S}_4 = \mathbf{Q}_0\mathbf{K}_F^\star\boldsymbol{\rho}_{LF}^{-1}\left(\mathbf{I}_F + \mathbf{k}_F^\star\boldsymbol{\rho}_{LF}\mathbf{K}_F^\star\boldsymbol{\rho}_{LF}^{-1}\right)^{-1}\mathbf{k}_F^\star\boldsymbol{\rho}_{LF}\mathbf{P}_0$$

are needed should one wish to obtain values of $\omega_0(z)$ on $\Gamma^\star$. Here $\mathbf{Q}_0$ is a discrete restriction operator in the opposite direction of $\mathbf{P}_0$.

5. Recursive construction of the $\mathbf{R}_m$ matrices. The computation of the four block diagonal matrices $\mathbf{R}_m$ of (4.14)–(4.17), directly from their definitions, is an expensive and unstable operation. The condition number of the matrix

$$\mathbf{I}_F^\star + \mathbf{k}_F^\star\boldsymbol{\rho}_{LF}\mathbf{K}_F^\star\boldsymbol{\rho}_{LF}^{-1}\,,$$

which has to be inverted, may grow exponentially with mesh refinement. The computational cost for direct inversion grows cubically. In contrast, the condition numbers of the final $\mathbf{R}_m$ matrices are often moderate. This section shows how to construct the $\mathbf{R}_m$ matrices in a fast and stable fashion.

The four matrix blocks associated with a particular $\Gamma_j^{\star\mathrm{bp}}$ or $\Gamma_l^{\star\mathrm{cp}}$ in the $\mathbf{R}_m$ matrices can be constructed simultaneously and independently of all other matrix blocks in a manner that lends itself well to parallelization. The procedure can be described with the same formalism for both types of curve segments. The chief differences are the size of the blocks and the complexity of the illustrations of various meshes. For simplicity in the derivation, we therefore concentrate on the four 64×64 blocks of the $\mathbf{R}_m$ matrices associated with a curve segment $\Gamma^{\star\mathrm{cp}}$ around a generic corner point.

5.1. Hierarchies of grids and matrices. Consider a coarse mesh on a curve segment $\Gamma^{\star\mathrm{cp}}$; see the upper left image of Figure 5.1. Let this mesh be n-ply refined so that there are $2(n+2)$ panels on $\Gamma^{\star\mathrm{cp}}$. The panel placement of a 5-ply refined mesh is shown in the lower left image of Figure 5.1.

Different grids on subsets of $\Gamma^{\star\mathrm{cp}}$ are introduced. Let $\Gamma_i^\star$ denote the part of $\Gamma^{\star\mathrm{cp}}$ covering a mesh made up of the $2(i+2)$ innermost panels, $1 \le i \le n$. Let $\mathcal{G}_{ia}$ denote a grid of $32(i+2)$ quadrature points τ_j on this i-ply refined mesh. The right images of Figure 5.1 show $\Gamma_i^\star$ for $i = 4$ and $n = 5$, and the upper right image is the mesh
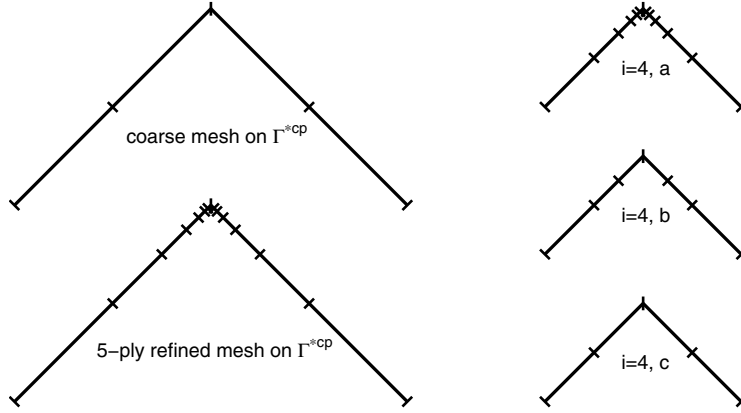
FIG. 5.1. *Placement of panels on* $\Gamma^{\star \mathrm{cp}}$. *Upper left: Panels of the coarse mesh. Lower left: Panels of an n-ply refined mesh, $n = 5$. Right: Panels on $\Gamma_i^\star$ upon which the grids $\mathcal{G}_{i\mathrm{a}}$, $\mathcal{G}_{i\mathrm{b}}$, and $\mathcal{G}_{i\mathrm{c}}$ are constructed for $i = 4$ and $n = 5$. Note that $\mathcal{G}_{i\mathrm{a}}$ and $\mathcal{G}_{i\mathrm{b}}$ coincide for $i = 1$.*

upon which $\mathcal{G}_{i\mathrm{a}}$ is constructed. Let $\mathcal{G}_{i\mathrm{b}}$ denote a grid of 96 quadrature points on a simply refined mesh on $\Gamma_i^\star$; see the middle right image. Let $\mathcal{G}_{i\mathrm{c}}$ denote a grid of 64 quadrature points on an unrefined mesh on $\Gamma_i^\star$; see the lower right image.

Families of matrices corresponding to discretizations of I, K, k, and ρ_{L} on $\mathcal{G}_{i\mathrm{a}}$ and $\mathcal{G}_{i\mathrm{b}}$ are needed. Let the subscript "$i\mathrm{a}$" refer to $32(i+2) \times 32(i+2)$ matrices corresponding to discretizations on $\mathcal{G}_{i\mathrm{a}}$. Let the subscript "$i\mathrm{b}$" refer to 96×96 matrices corresponding to discretizations on $\mathcal{G}_{i\mathrm{b}}$.

We also need discrete prolongation operators, in the style of section 4.3, between the grids. For each quadrature point τ_j in $\mathcal{G}_{i\mathrm{a}}$, $\mathcal{G}_{i\mathrm{b}}$, and $\mathcal{G}_{i\mathrm{c}}$ there are corresponding quadrature weights w_{1j} and w_{2j}. Let $\mathbf{W}_{lix}$, $l = 1, 2$, $x = a, b, c$, be six diagonal matrices constructed from these weights in accordance with (4.5). Let $\mathbf{P}_{0i\mathrm{ab}}$ be the prolongation operator that performs polynomial interpolation from $\mathcal{G}_{i\mathrm{b}}$ to $\mathcal{G}_{i\mathrm{a}}$. Let

$$(5.1) \qquad \mathbf{P}_{li\mathrm{ab}} = \mathbf{W}_{li\mathrm{a}} \mathbf{P}_{0i\mathrm{ab}} \mathbf{W}_{li\mathrm{b}}^{-1}, \quad l = 1, 2.$$

Define $\mathbf{P}_{li\mathrm{ac}}$, and $\mathbf{P}_{li\mathrm{bc}}$, $l = 0, 1, 2$, in a similar fashion.

Useful relations that follow from the definitions above are

$$(5.2) \qquad \mathbf{P}_{li\mathrm{ac}} = \mathbf{P}_{li\mathrm{ab}} \mathbf{P}_{l\mathrm{bc}}, \quad l = 0, 1, 2,$$

$$(5.3) \qquad \mathbf{P}_{li\mathrm{ab}}^T \mathbf{P}_{0i\mathrm{ab}} = \mathbf{I}_{\mathrm{b}}, \quad l = 1, 2,$$

where we have dropped the index i from matrices that are independent of i, and (5.3) holds in the same sense as (4.8). Relation (5.2) says that (weighted) polynomial interpolation from a coarser to a finer grid can be done via a medium fine grid.

Now define the four families of 64×64 matrices $\mathbf{R}_{mi}$, $m = 1, 2, 3, 4$, as

$$(5.4) \quad \mathbf{R}_{1i} = \mathbf{P}_{1i\mathrm{ac}}^T \left(\mathbf{I}_{i\mathrm{a}} + \mathbf{k}_{i\mathrm{a}} \boldsymbol{\rho}_{\mathrm{L}i\mathrm{a}} \mathbf{K}_{i\mathrm{a}} \boldsymbol{\rho}_{\mathrm{L}i\mathrm{a}}^{-1} \right)^{-1} \mathbf{P}_{0i\mathrm{ac}}, \qquad i = 1, \ldots, n,$$

$$(5.5) \quad \mathbf{R}_{2i} = \mathbf{P}_{2i\mathrm{ac}}^T \mathbf{K}_{i\mathrm{a}} \boldsymbol{\rho}_{\mathrm{L}i\mathrm{a}}^{-1} \left(\mathbf{I}_{i\mathrm{a}} + \mathbf{k}_{i\mathrm{a}} \boldsymbol{\rho}_{\mathrm{L}i\mathrm{a}} \mathbf{K}_{i\mathrm{a}} \boldsymbol{\rho}_{\mathrm{L}i\mathrm{a}}^{-1} \right)^{-1} \mathbf{P}_{0i\mathrm{ac}}, \qquad i = 1, \ldots, n,$$

$$(5.6) \quad \mathbf{R}_{3i} = \mathbf{P}_{1i\mathrm{ac}}^T \left(\mathbf{I}_{i\mathrm{a}} + \mathbf{k}_{i\mathrm{a}} \boldsymbol{\rho}_{\mathrm{L}i\mathrm{a}} \mathbf{K}_{i\mathrm{a}} \boldsymbol{\rho}_{\mathrm{L}i\mathrm{a}}^{-1} \right)^{-1} \mathbf{k}_{i\mathrm{a}} \boldsymbol{\rho}_{\mathrm{L}i\mathrm{a}} \mathbf{P}_{0i\mathrm{ac}}, \qquad i = 1, \ldots, n,$$

$$(5.7) \quad \mathbf{R}_{4i} = \mathbf{P}_{2i\mathrm{ac}}^T \mathbf{K}_{i\mathrm{a}} \boldsymbol{\rho}_{\mathrm{L}i\mathrm{a}}^{-1} \left(\mathbf{I}_{i\mathrm{a}} + \mathbf{k}_{i\mathrm{a}} \boldsymbol{\rho}_{\mathrm{L}i\mathrm{a}} \mathbf{K}_{i\mathrm{a}} \boldsymbol{\rho}_{\mathrm{L}i\mathrm{a}}^{-1} \right)^{-1} \mathbf{k}_{i\mathrm{a}} \boldsymbol{\rho}_{\mathrm{L}i\mathrm{a}} \mathbf{P}_{0i\mathrm{ac}}, \qquad i = 1, \ldots, n.$$

The $\mathbf{R}_{mi}$ matrices with $i = n$ incorporate all discretization points on the n-ply refined mesh on $\Gamma^{\star\text{cp}}$, that is, $\mathcal{G}_{na}$. Therefore, the $\mathbf{R}_{mn}$ matrices correspond to the diagonal block of $\mathbf{R}_1$, $\mathbf{R}_2$, $\mathbf{R}_3$, and $\mathbf{R}_4$ in (4.14)–(4.17) associated with $\Gamma^{\star\text{cp}}$.

5.2. Splits and decompositions. We seek relations between the $\mathbf{R}_{mi}$ matrices of (5.4)–(5.7) with different indices. More precisely, we want to express the $\mathbf{R}_{mi}$ matrices in terms of the $\mathbf{R}_{m(i-1)}$ matrices and quantities which can be cheaply computed on the small grids $\mathcal{G}_{ib}$. This will result in a fast recursion for $\mathbf{R}_{mn}$. We must eliminate all quantities related to the large grids $\mathcal{G}_{ia}$.

Let $\mathbf{M}$ denote any of the matrices $\mathbf{k}$, $\mathbf{K}$, or $\mathbf{I}$, and let it be split as follows:

$$(5.8) \qquad \mathbf{M}_{ix} = \mathbf{M}_{ix}^{\star} + \mathbf{M}_{ix}^{\circ}, \qquad x = \text{a}, \text{b}, \quad i = 1, \ldots, n.$$

Here $\mathbf{M}_{ia}^{\star}$ contains the elements of $\mathbf{M}_{ia}$ with both indices in the set $\{17 : 32i + 48\}$, the remaining elements being zero. $\mathbf{M}_{ia}^{\circ}$ contains the elements of $\mathbf{M}_{ia}$ with at least one index in the set $\{1 : 16\}$ or $\{32i + 49 : 32(i + 2)\}$, the remaining elements being zero. $\mathbf{M}_{ib}^{\star}$ contains the elements of $\mathbf{M}_{ib}$ with both indices in the set $\{17 : 80\}$, the remaining elements being zero. $\mathbf{M}_{ib}^{\circ}$ contains the elements of $\mathbf{M}_{ib}$ with at least one index in the set $\{1 : 16\}$ or $\{81 : 96\}$, the remaining elements being zero.

One can view the nonzero elements of $\mathbf{M}_{ia}^{\circ}$ and $\mathbf{M}_{ib}^{\circ}$ as frames of width 16 around the nonzero elements of $\mathbf{M}_{ia}^{\star}$ and $\mathbf{M}_{ib}^{\star}$. Let $\mathbb{F}\{\cdot\}$ denote an operator which creates a frame of width 16 of zeros around its argument. Then

$$(5.9) \qquad \mathbf{M}_{ia}^{\star} = \mathbb{F}\{\mathbf{M}_{(i-1)a}\}, \quad i = 2, \ldots, n.$$

The following relations are a consequence of the sparsity pattern of $\mathbf{M}^{\star}$ and $\mathbf{M}^{\circ}$:

$$(5.10) \qquad \mathbf{M}^{\star}\mathbf{M}^{\circ}\mathbf{M}^{\star} = 0,$$

$$(5.11) \qquad (\mathbf{I} + \mathbf{M}^{\star}\mathbf{M}^{\circ})^{-1} = \mathbf{I} - \mathbf{M}^{\star}\mathbf{M}^{\circ}.$$

The matrices $\mathbf{k}_{ia}^{\circ}\boldsymbol{\rho}_{Lia}$ and $\mathbf{K}_{ia}^{\circ}\boldsymbol{\rho}_{Lia}^{-1}$ have interesting spectral properties. They have low rank, essentially independent of the values of n and i. In addition, $\mathbf{k}_{ia}^{\circ}\boldsymbol{\rho}_{Lia}$ typically has a small spectral radius. One consequence of the low rank property is that the decompositions

$$(5.12) \qquad \mathbf{k}_{ia}^{\circ}\boldsymbol{\rho}_{Lia} = \mathbf{P}_{0iab}\mathbf{k}_{ib}^{\circ}\boldsymbol{\rho}_{Lib}\mathbf{P}_{2iab}^{T},$$

$$(5.13) \qquad \mathbf{K}_{ia}^{\circ}\boldsymbol{\rho}_{Lia}^{-1} = \mathbf{P}_{0iab}\mathbf{K}_{ib}^{\circ}\boldsymbol{\rho}_{Lib}^{-1}\mathbf{P}_{1iab}^{T},$$

where the right-hand sides involve prolongation of off-diagonal matrix blocks, hold to high accuracy. Useful relations that follow from (5.3), (5.8), (5.12), and (5.13) are

$$(5.14) \qquad \mathbf{P}_{2iab}^{T}\mathbf{K}_{ia}\boldsymbol{\rho}_{Lia}^{-1} = \mathbf{P}_{2iab}^{T}\mathbf{K}_{ia}^{\star}\boldsymbol{\rho}_{Lia}^{-1} + \mathbf{K}_{ib}^{\circ}\boldsymbol{\rho}_{Lib}^{-1}\mathbf{P}_{1iab}^{T},$$

$$(5.15) \qquad \mathbf{k}_{ia}\boldsymbol{\rho}_{Lia}\mathbf{P}_{0iab} = \mathbf{k}_{ia}^{\star}\boldsymbol{\rho}_{Lia}\mathbf{P}_{0iab} + \mathbf{P}_{0iab}\mathbf{k}_{ib}^{\circ}\boldsymbol{\rho}_{Lib}.$$

We shall temporarily work with $\mathbf{R}_{mi}$ as a general expression

$$(5.16) \qquad \mathbf{R}_{mi} = \mathbf{P}_{liac}^{T}\mathbf{X}_{ia}\left(\mathbf{I}_{ia} + \mathbf{k}_{ia}\boldsymbol{\rho}_{Lia}\mathbf{K}_{ia}\boldsymbol{\rho}_{Lia}^{-1}\right)^{-1}\mathbf{Y}_{ia}\mathbf{P}_{0iac},$$

from which (5.4)–(5.7) are obtained by choosing $\mathbf{X}$ as $\mathbf{I}$ or $\mathbf{K}\boldsymbol{\rho}_{L}^{-1}$, $\mathbf{Y}$ as $\mathbf{I}$ or $\mathbf{k}\boldsymbol{\rho}_{L}$, and l as 1 or 2 depending on m. With (5.2), (5.3), and the split (5.8) for $\mathbf{k}_{ia}$, one can write

$$(5.17)$$
$$\mathbf{R}_{mi} = \mathbf{P}_{lbc}^{T}\mathbf{P}_{liab}^{T}\mathbf{X}_{ia}\left(\mathbf{I}_{ia} + \mathbf{k}_{ia}^{\star}\boldsymbol{\rho}_{Lia}\mathbf{K}_{ia}\boldsymbol{\rho}_{Lia}^{-1} + \mathbf{k}_{ia}^{\circ}\boldsymbol{\rho}_{Lia}\mathbf{K}_{ia}\boldsymbol{\rho}_{Lia}^{-1}\right)^{-1}\mathbf{Y}_{ia}\mathbf{P}_{0iab}\mathbf{P}_{0bc}.$$

The spectral radius of the matrix

$$(5.18) \qquad \mathbf{k}_{ia}^{\circ}\boldsymbol{\rho}_{Lia}\mathbf{K}_{ia}\boldsymbol{\rho}_{Lia}^{-1}\left(\mathbf{I}_{ia} + \mathbf{k}_{ia}^{\star}\boldsymbol{\rho}_{Lia}\mathbf{K}_{ia}\boldsymbol{\rho}_{Lia}^{-1}\right)^{-1}$$

is well below unity thanks to the spectral properties of $\mathbf{k}_{ia}^{\circ}\boldsymbol{\rho}_{Lia}$. A typical value in the numerical examples of section 7 is 0.2. This makes it possible to expand (5.17) in a Neumann series. After substituting (5.12) into this series it can be brought back in closed form:

$$(5.19) \quad \mathbf{R}_{mi} = \mathbf{P}_{lbc}^{T}\Big(\mathbf{G}_{lia}(\mathbf{X},\mathbf{Y}) - \mathbf{G}_{lia}(\mathbf{X},\mathbf{I})\left(\mathbf{I}_{b} + \mathbf{k}_{ib}^{\circ}\boldsymbol{\rho}_{Lib}\mathbf{G}_{2ia}(\mathbf{K}\boldsymbol{\rho}_{L}^{-1},\mathbf{I})\right)^{-1}$$
$$\times \mathbf{k}_{ib}^{\circ}\boldsymbol{\rho}_{Lib}\mathbf{G}_{2ia}(\mathbf{K}\boldsymbol{\rho}_{L}^{-1},\mathbf{Y})\Big)\mathbf{P}_{0bc}\,,$$

where the abbreviation

$$(5.20) \qquad \mathbf{G}_{lia}(\mathbf{X},\mathbf{Y}) = \mathbf{P}_{liab}^{T}\mathbf{X}_{ia}\left(\mathbf{I}_{ia} + \mathbf{k}_{ia}^{\star}\boldsymbol{\rho}_{Lia}\mathbf{K}_{ia}\boldsymbol{\rho}_{Lia}^{-1}\right)^{-1}\mathbf{Y}_{ia}\mathbf{P}_{0iab}$$

is introduced. With (5.3), (5.10), (5.11), (5.13), and the split (5.8) for $\mathbf{K}_{ia}$, one can write

$$(5.21) \quad \mathbf{G}_{lia}(\mathbf{X},\mathbf{Y}) = \mathbf{P}_{liab}^{T}\mathbf{X}_{ia}\left(\mathbf{I}_{ia} + \mathbf{k}_{ia}^{\star}\boldsymbol{\rho}_{Lia}\mathbf{K}_{ia}^{\star}\boldsymbol{\rho}_{Lia}^{-1}\right)^{-1}\mathbf{Y}_{ia}\mathbf{P}_{0iab}$$
$$- \mathbf{P}_{liab}^{T}\mathbf{X}_{ia}\left(\mathbf{I}_{ia} + \mathbf{k}_{ia}^{\star}\boldsymbol{\rho}_{Lia}\mathbf{K}_{ia}^{\star}\boldsymbol{\rho}_{Lia}^{-1}\right)^{-1}\mathbf{k}_{ia}^{\star}\boldsymbol{\rho}_{Lia}\mathbf{P}_{0iab}\mathbf{K}_{ib}^{\circ}\boldsymbol{\rho}_{Lib}^{-1}\mathbf{Y}_{ib}^{\circ}\,.$$

5.3. Fast recursion for $\mathbf{R}_{mn}$. Written out explicitly, the $\mathbf{R}_{mi}$ of (5.19) become

$$(5.22) \qquad \mathbf{R}_{1i} = \mathbf{P}_{1bc}^{T}\mathbf{A}_{i}\left(\mathbf{I}_{b} + \mathbf{k}_{ib}^{\circ}\boldsymbol{\rho}_{Lib}\mathbf{B}_{i}\right)^{-1}\mathbf{P}_{0bc}\,,$$

$$(5.23) \qquad \mathbf{R}_{2i} = \mathbf{P}_{2bc}^{T}\mathbf{B}_{i}\left(\mathbf{I}_{b} + \mathbf{k}_{ib}^{\circ}\boldsymbol{\rho}_{Lib}\mathbf{B}_{i}\right)^{-1}\mathbf{P}_{0bc}\,,$$

$$(5.24) \qquad \mathbf{R}_{3i} = \mathbf{P}_{1bc}^{T}\left(\mathbf{C}_{i} - \mathbf{A}_{i}\left(\mathbf{I}_{b} + \mathbf{k}_{ib}^{\circ}\boldsymbol{\rho}_{Lib}\mathbf{B}_{i}\right)^{-1}\mathbf{k}_{ib}^{\circ}\boldsymbol{\rho}_{Lib}\mathbf{D}_{i}\right)\mathbf{P}_{0bc}\,,$$

$$(5.25) \qquad \mathbf{R}_{4i} = \mathbf{P}_{2bc}^{T}\left(\mathbf{D}_{i} - \mathbf{B}_{i}\left(\mathbf{I}_{b} + \mathbf{k}_{ib}^{\circ}\boldsymbol{\rho}_{Lib}\mathbf{B}_{i}\right)^{-1}\mathbf{k}_{ib}^{\circ}\boldsymbol{\rho}_{Lib}\mathbf{D}_{i}\right)\mathbf{P}_{0bc}\,,$$

where

$$(5.26) \qquad\qquad \mathbf{A}_{i} = \mathbf{G}_{1ia}(\mathbf{I},\mathbf{I})\,,$$

$$(5.27) \qquad\qquad \mathbf{B}_{i} = \mathbf{G}_{2ia}(\mathbf{K}\boldsymbol{\rho}_{L}^{-1},\mathbf{I})\,,$$

$$(5.28) \qquad\qquad \mathbf{C}_{i} = \mathbf{G}_{1ia}(\mathbf{I},\mathbf{k}\boldsymbol{\rho}_{L})\,,$$

$$(5.29) \qquad\qquad \mathbf{D}_{i} = \mathbf{G}_{2ia}(\mathbf{K}\boldsymbol{\rho}_{L}^{-1},\mathbf{k}\boldsymbol{\rho}_{L})\,.$$

One can now express $\mathbf{A}_{i}$, $\mathbf{B}_{i}$, $\mathbf{C}_{i}$, and $\mathbf{D}_{i}$ via (5.21) solely in terms of $\mathbf{R}_{m(i-1)}$, $\mathbf{k}_{ib}^{\circ}\boldsymbol{\rho}_{Lib}$, and $\mathbf{K}_{ib}^{\circ}\boldsymbol{\rho}_{Lib}^{-1}$. Simply insert the appropriate expressions for $\mathbf{X}$ and $\mathbf{Y}$ in (5.21) and use (5.9), (5.14), and (5.15) to obtain

$$(5.30) \qquad\qquad \mathbf{A}_{i} = \mathbb{F}\{\mathbf{R}_{1(i-1)}\} + \mathbf{I}_{b}^{\circ} - \mathbb{F}\{\mathbf{R}_{3(i-1)}\}\mathbf{K}_{ib}^{\circ}\boldsymbol{\rho}_{Lib}^{-1}\,,$$

$$(5.31) \qquad\qquad \mathbf{B}_{i} = \mathbb{F}\{\mathbf{R}_{2(i-1)}\} + \mathbf{K}_{ib}^{\circ}\boldsymbol{\rho}_{Lib}^{-1}\mathbf{A}_{i} - \mathbb{F}\{\mathbf{R}_{4(i-1)}\}\mathbf{K}_{ib}^{\circ}\boldsymbol{\rho}_{Lib}^{-1}\,,$$

$$(5.32) \qquad\qquad \mathbf{C}_{i} = \mathbb{F}\{\mathbf{R}_{3(i-1)}\} + \mathbf{A}_{i}\mathbf{k}_{ib}^{\circ}\boldsymbol{\rho}_{Lib}\,,$$

$$(5.33) \qquad\qquad \mathbf{D}_{i} = \mathbb{F}\{\mathbf{R}_{4(i-1)}\} + \mathbf{B}_{i}\mathbf{k}_{ib}^{\circ}\boldsymbol{\rho}_{Lib} + \mathbf{K}_{ib}^{\circ}\boldsymbol{\rho}_{Lib}^{-1}\mathbb{F}\{\mathbf{R}_{3(i-1)}\}\,.$$

Equations (5.22)–(5.25), for $i = 1, \ldots, n$, together with (5.30)–(5.33) constitute the recursion sought in this section. It can be initialized as

$$(5.34) \qquad \mathbb{F}\{\mathbf{R}_{10}\} = \left(\mathbf{I}_{\mathrm{b}}^{\star} + \mathbf{k}_{1\mathrm{b}}^{\star}\boldsymbol{\rho}_{\mathrm{L1b}}\mathbf{K}_{1\mathrm{b}}^{\star}\boldsymbol{\rho}_{\mathrm{L1b}}^{-1}\right)^{-1},$$

$$(5.35) \qquad \mathbb{F}\{\mathbf{R}_{20}\} = \mathbf{K}_{1\mathrm{b}}^{\star}\boldsymbol{\rho}_{\mathrm{L1b}}^{-1}\mathbb{F}\{\mathbf{R}_{10}\},$$

$$(5.36) \qquad \mathbb{F}\{\mathbf{R}_{30}\} = \mathbb{F}\{\mathbf{R}_{10}\}\mathbf{k}_{1\mathrm{b}}^{\star}\boldsymbol{\rho}_{\mathrm{L1b}},$$

$$(5.37) \qquad \mathbb{F}\{\mathbf{R}_{40}\} = \mathbf{K}_{1\mathrm{b}}^{\star}\boldsymbol{\rho}_{\mathrm{L1b}}^{-1}\mathbb{F}\{\mathbf{R}_{30}\}.$$

6. Applications. So far we have reduced, transformed, and discretized the original singular system (2.5), (2.6). The purpose was to get a formulation better suited for numerical computations. We have also shown how to construct various auxiliary quantities in a fast and stable fashion. The result is the consolidated compressed equation (4.20) together with the recursion (5.22)–(5.25), (5.30)–(5.33). The curve Γ, the dominant operator K, and the fundamental function $\rho(z)$ were specified in section 2. In order to demonstrate the numerical efficiency of our proposed scheme, we must now make a particular choice of the operator k and the right-hand side $g(z)$. We choose an application to planar crack problems since such problems are the motivating force behind this work. This section contains a brief review of crack problems with focus on k and on $g(z)$. We also introduce a functional F of the solution $\omega_0(z)$, which is of importance in fracture mechanics and can serve as a measure of convergence. The presentation follows [9, 20] and the references therein.

6.1. The elastostatic crack problem. Consider an infinite elastic plane with stress

$$(6.1) \qquad \lim_{z \to \infty} (\sigma_{xx}(z), \sigma_{yy}(z), \sigma_{xy}(z)) = (\sigma_{xx}^{\infty}, \sigma_{yy}^{\infty}, \sigma_{xy}^{\infty})$$

applied at infinity. Let the plane be cut along a connected curve Γ of the type discussed in section 2.2. Such a curve will be called a crack, and its p endpoints γ_i^{ep} are crack tips. The crack is free of traction on its faces and is allowed to respond to external loading with any finite opening displacement. The problem of determining the stress- and displacement fields in this plane is a linear elastostatic problem. The stress state at infinity may be described in terms of two constants α and β via $\sigma_{xx}^{\infty} + \sigma_{yy}^{\infty} = 2\alpha$ and $\sigma_{yy}^{\infty} - \sigma_{xx}^{\infty} + 2\mathrm{i}\sigma_{xy}^{\infty} = 2\bar{\beta}$, where "bar" is the complex conjugate.

The normalized complex valued stress intensity factor F at crack tip γ_i^{ep} is

$$(6.2) \qquad F(\gamma_i^{\mathrm{ep}}) = \lim_{\epsilon \to 0+} \frac{\sqrt{2\epsilon}}{\sigma^{\infty}\sqrt{c}} \left[\sigma_{y'y'}(\gamma_i^{\mathrm{ep}} \mp \mathrm{i}\epsilon n(\gamma_i^{\mathrm{ep}})) + \mathrm{i}\sigma_{x'y'}(\gamma_i^{\mathrm{ep}} \mp \mathrm{i}\epsilon n(\gamma_i^{\mathrm{ep}}))\right],$$

where ϵ is a real number, x' and y' refer to local coordinate systems aligned with the crack at the tip, σ^{∞} is related to the applied load, c is a geometry dependent constant, and the sign depends on the orientation of Γ. Stress intensity factors can be computed once the elastostatic problem is solved. They are of interest in the study of fracture processes [11].

6.2. A singular integral equation. Singular integral equations for the elastostatic crack problem can be derived from potential representations of stress- or displacement fields. We choose a stress-based formulation, omit the derivation, and simply state results.

The stress field in the plane can be computed from a layer density $\omega_0(z)$ on Γ determined by the system (2.5), (2.6) with K and $\rho(z)$ as in section 2, with a right-hand side

$$(6.3) \qquad g(z) = -\alpha + \bar{\beta}\frac{\bar{n}_z}{n_z},$$

and with an operator k whose action on a function $\omega(z)$ is given by

$$(6.4) \quad k\omega(z) = -\frac{1}{2\pi i}\left[\int_\Gamma \frac{\omega(\tau)\,d\tau}{\tau - z} + \frac{\bar{n}_z}{n_z}\int_\Gamma \frac{\omega(\tau)\,d\tau}{\bar{\tau} - \bar{z}}\right.$$
$$\left. + \int_\Gamma \frac{\overline{\omega(\tau)}\,d\bar{\tau}}{\bar{\tau} - \bar{z}} + \frac{\bar{n}_z}{n_z}\int_\Gamma \frac{(\tau - z)\overline{\omega(\tau)}\,d\bar{\tau}}{(\bar{\tau} - \bar{z})^2}\right], \quad z \in \Gamma.$$

The kernel $k(\tau, z)$ of the operator k in (6.4) can be viewed as made up of two parts—one that acts on $\omega(z)$ and one that acts on the conjugate of $\omega(z)$. Both parts have computable limits for $\tau \to z$, so $k(\tau, z)$ is smooth on smooth curves as required in section 1.1. The operator $k\rho$ can be discretized using basic quadrature with weights w_{2i}; see section 4.1. Note that complex linear systems containing a mix of conjugated and nonconjugated unknowns may, strictly speaking, not be linear. But if expanded into real systems of twice the size, the linearity property is retained. Inverses of matrices containing $\mathbf{k}\boldsymbol{\rho}$ should be interpreted with this in mind.

Once the reduced equation (2.7) with the choices (6.3) and (6.4) is solved for $\Omega(z)$, the density ω_0 can be recovered via (2.8) and several quantities of physical interest can be computed. In particular, the normalized stress intensity factors follow from

$$(6.5) \qquad F(\gamma_i^{\text{ep}}) = \pm\frac{i\sqrt{2}}{\sigma^\infty\sqrt{c}}\overline{\omega_0(\gamma_i^{\text{ep}})}\lim_{z\to\gamma_i^{\text{ep}}}\overline{\rho(z)}\sqrt{\delta s(z)}, \quad z \in \Gamma,$$

where $\delta s(z)$ is arc length measured from the closest crack tip.

7. Numerical examples. We seek $\boldsymbol{\omega}_0$, a discretization of the density $\omega_0(z)$ which solves the system (2.5), (2.6) for the choices made in section 6. Two schemes will be compared for a variety of increasingly complex cracks Γ:

(I) Solve the reduced equation (4.4) for $\boldsymbol{\Omega}_{\text{F}}$ on an n-ply refined mesh. Compute $\boldsymbol{\omega}_{0\text{F}}$ from $\boldsymbol{\Omega}_{\text{F}}$ via a discrete version of (2.8).

(II) Solve the compressed equation (4.20) for $\hat{\boldsymbol{\Omega}}_{\text{C}}$ with n steps per $\Gamma_j^{\star\text{bp}}$ and $\Gamma_l^{\star\text{cp}}$ in the recursion (5.22)–(5.25), (5.30)–(5.33). Compute $\boldsymbol{\omega}_{0\text{C}}$ from $\hat{\boldsymbol{\Omega}}_{\text{C}}$ via (4.21).

As a check for convergence, we evaluate $F(\gamma_i^{\text{ep}})$, for some i, from a discretized version of (6.5). Here 15th-degree polynomial extrapolation of $\boldsymbol{\omega}_0$ is used on panels neighboring the γ_i^{ep}, since endpoints are not quadrature points.

The numerical experiments are performed in MATLAB version 7.6 and executed on an ordinary workstation equipped with an IntelCore2 Duo E8400 CPU at 3.00 GHz and 4GB of memory. The GMRES iterative solver [28] with a low-threshold stagnation avoiding technique [19] is used for the main linear systems. System matrices and their action on vectors are computed explicitly for the smaller problems. The fast multipole method [13, 14] is used for the larger problems.

7.1. The V-shaped crack. The boundary Γ is that of the V-shaped crack in an elastic plane depicted in the left image of Figure 2.1. The stress state at infinity corresponds to uniaxial loading and is given by $\alpha = \beta = 0.5$ so that $\sigma_{yy}^\infty = 1$. The coarse

TABLE 7.1

Normalized stress intensity factors $F(\gamma_1^{\text{ep}}) = F_{\text{I}} + iF_{\text{II}}$ of (6.2) with $\sigma^\infty = \sigma_{yy}^\infty$ for zigzag-shaped cracks with q corners under loading given by $\alpha = \beta = 0.5$. The constant c is half the distance between γ_1^{ep} and γ_2^{ep}, that is, $c = \mathtt{a}$. The V-shaped crack has $q = 1$. Digits within parentheses are uncertain.

Number of corners q	F_{I}: our reference solution	F_{II}: our reference solution
1	0.52076755221826(35)	0.64111594549615(34)
7	0.64474534910119(81)	0.47836718562682(08)
19	0.69741383867475(43)	0.41737553644506(84)
199	0.7653969177868(94)	0.3430397840877(62)
1999	0.788301598079(95)	0.318844942843(65)
19999	0.79568696939(67)	0.31111845739(16)

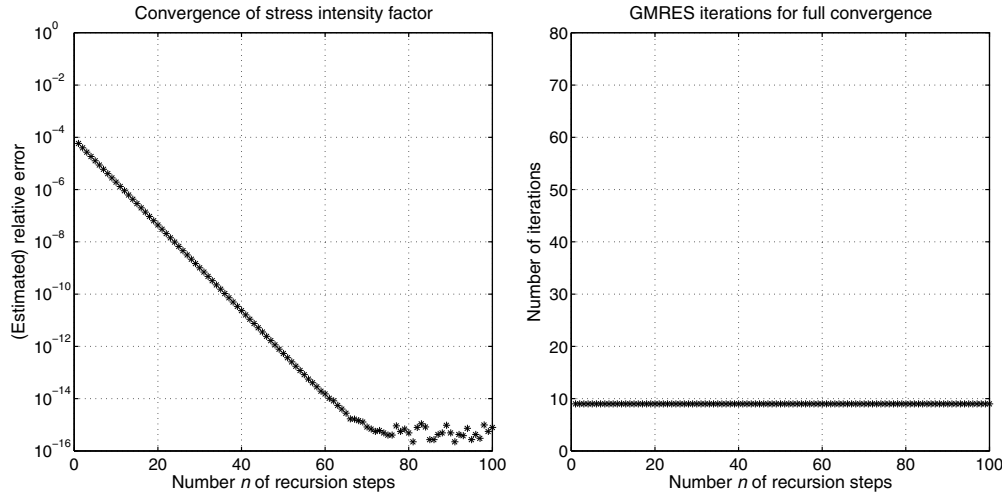| Corners q	F_{I}: from [7, 8]	F_{II}: from [8]	$F_{\text{I}}/F_{\text{II}}$: from [2]	$F_{\text{I}}/F_{\text{II}}$: from [30]
1	0.5207675522	0.6411159455	0.520/0.641	0.520767/0.641117
7	0.644745		0.652/0.470	
19	0.697413839	0.417375537		
199	0.76539692	0.34303978		
1999	0.7883016	0.3188449		

FIG. 7.1. *The V-shaped crack. Convergence of the stress intensity factor $F(\gamma_1^{\text{ep}})$ of (6.2). Scheme* (II) *is used. The main linear system has* 128 *unknowns irrespective of the number n of recursion steps. The reference solution is taken from Table* 7.1. *Compare Figure* 1.1.

mesh has eight quadrature panels, which is more than enough to resolve $\Omega(z)$ on $\Gamma \setminus \Gamma^\star$. This means that $\boldsymbol{\Omega}_{\text{F}}$ is represented by $32(4 + n)$ unknown discrete values in scheme (I) and that $\hat{\boldsymbol{\Omega}}_{\text{C}}$ is represented by 128 unknown discrete values in scheme (II).

Values of $F(\gamma_1^{\text{ep}})$ for this crack have been computed before [2, 7, 8, 30]. Previous results, converged to between three and ten digits, and new results are summarized in Table 7.1. The performance of scheme (I) is shown in Figure 1.1 of section 1. The computational time grows with refinement level n as follows: $n = 20$ takes 0.71 seconds; $n = 40$ takes 2.4 seconds; $n = 60$ takes 6.1 seconds; and $n = 80$ takes 12.3 seconds. The linear systems used in [30] needed between 7 and 97 seconds for their solution.

Figure 7.1 shows the result of scheme (II). The difference, compared to scheme (I) of Figure 1.1, is striking. Not only does the computed stress intensity factor converge

stably to an answer with an estimated relative error of 10^{-15}, the number of GMRES iterations needed for convergence is now only nine, irrespective of the number of recursion steps n. The computational time grows with the number of recursion steps roughly as follows: $n = 20$ takes 0.37 seconds; $n = 40$ takes 0.68 seconds; $n = 60$ takes 0.98 seconds; and $n = 80$ takes 1.29 seconds. This is in agreement with the complexity estimate $c_0 + O(\log E_0/E)$ claimed in section 1.6.

We conclude that the "complicated" scheme (II) outperforms the "simple" scheme (I) in the respects that matter most: stability and speed.
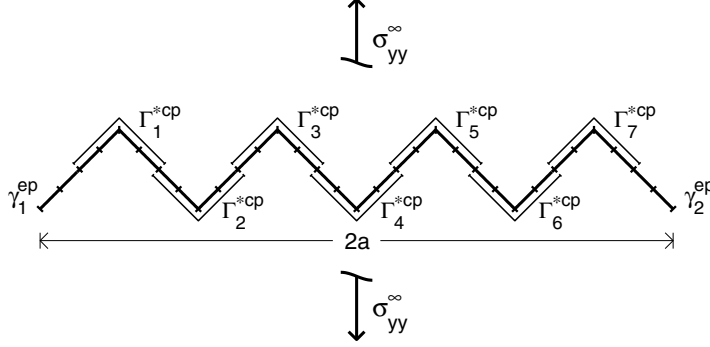
FIG. 7.2. *A zigzag-shaped crack with $q = 7$ right-angled corners made up of $q + 1$ straight line segments. There are four coarse quadrature panels placed on each segment. The curve segments where the recursion (5.22)–(5.25), (5.30)–(5.33) takes place are denoted $\Gamma_l^{\star cp}$, $l = 1, \ldots, q$.*

7.2. Zigzag-shaped cracks. The presence of more corner points on a crack Γ poses no problems for our new scheme (II) as it stands. If Γ consists of straight line segments and many corners have identical opening angles, additional savings in both execution time and storage are possible. It suffices to compute the four blocks of the $\mathbf{R}_m$ matrices associated with a corner with a given opening angle just once.

Figure 7.2 shows a zigzag-shaped crack with $q = 7$ corners. A coarse mesh with four panels per straight line segment is also shown along with the location of the disjoint curve segments $\Gamma_l^{\star cp}$, where the recursion takes place. Two results for the stress intensity factor $F(\gamma_1^{ep})$ of this crack were found in the literature. See Table 7.1.

Figure 7.3 shows convergence for both schemes. Two coarse meshes are used in conjunction with scheme (II)—one mesh with four panels per straight segment, corresponding to 512 unknowns in (4.20), and one mesh with eight panels per straight line segment, corresponding to 1024 unknowns. The right image of Figure 7.3 demonstrates that four coarse panels per segment is sufficient for full resolution on $\Gamma \setminus \Gamma^\star$.

By comparing Figure 7.3 to the left images of Figures 1.1 and 7.1, one can see that the zigzag-shaped crack, while still simple, is harder to resolve on $\Gamma^\star$ than the V-shaped crack. At a given level of mesh refinement, or with a given number of recursion steps, the error for the zigzag-shaped crack is about 25 times larger than for the V-shaped crack. Furthermore, with more than $n = 41$ subdivisions, the scheme (I) breaks down due to limitations of finite precision arithmetic. This illustrates the point made in section 1.4, that increased geometric difficulty poses tougher challenges to algorithms, and that precision can be lost quickly. Fortunately, scheme (II) converges as stably for the zigzag-shaped crack as for the V-shaped crack. The number of GMRES iterations needed for full convergence is now 18, irrespective of the number of recursion steps.
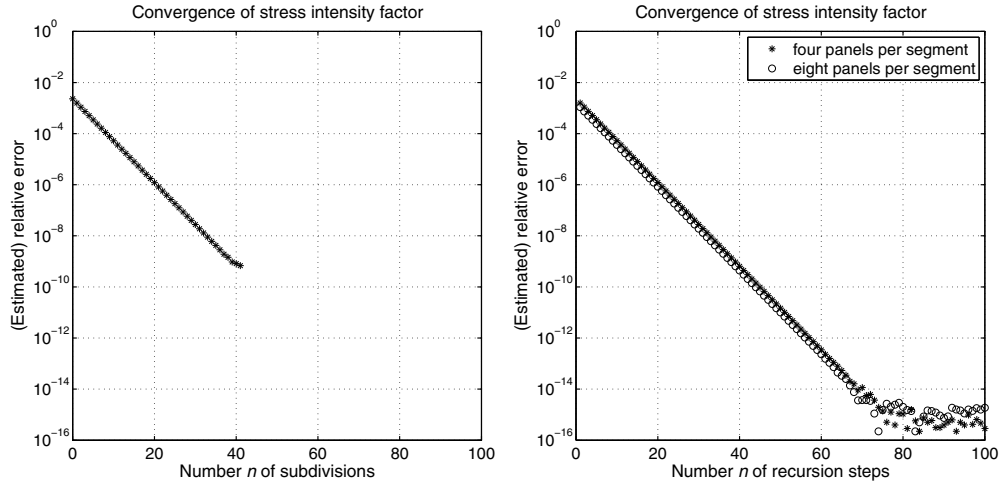
FIG. 7.3. *The zigzag-shaped crack with* $q = 7$ *corners. Convergence of the stress intensity factor* $F(\gamma_1^{\mathrm{ep}})$ *of* (6.2). *Left: scheme* (I) *with* $512 + 224n$ *unknowns in the main linear system. Right: scheme* (II) *with* 512 *or* 1024 *unknowns. The reference solution is taken from Table* 7.1.
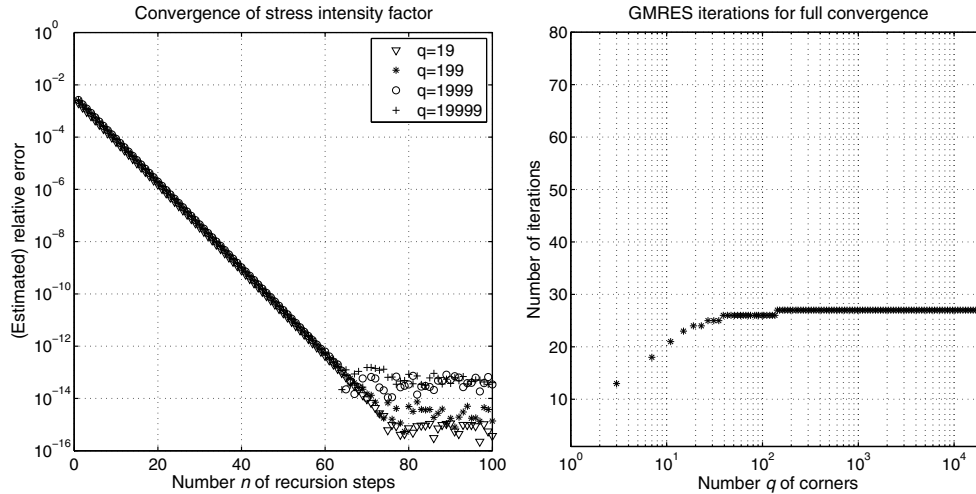

FIG. 7.4. *Zigzag-shaped cracks with varying numbers* q *of corners. Left: Convergence of* $F(\gamma_1^{\mathrm{ep}})$ *for* $q = 19$, $q = 199$, $q = 1999$, *and* $q = 19999$. *The reference solutions are taken from Table* 7.1. *Right:* GMRES *iterations needed to reach* ϵ_{mach} *in the relative residual. The most complicated crack has* $q = 22931$ *corners. The number of recursion steps is* $n = 80$.

We also put scheme (II) to the test on some larger zigzag-shaped cracks. The geometry is, basically, that of Figure 7.2. But the number q of corners varies. The left image of Figure 7.4 shows convergence of $F(\gamma_1^{\mathrm{ep}})$ for $q = 19$, $q = 199$, $q = 1999$, and $q = 19999$ to a precision of approximately $q \cdot \epsilon_{\mathrm{mach}}$, that is, to the same accuracy with which the length of an individual straight line segment can be determined in finite precision arithmetic. Stress intensity factors for some of these cracks were also computed by Englund [8], using a reduced integral equation and a mix of mild local mesh refinement and special basis functions developed for right-angled corners. Convergence of $F(\gamma_1^{\mathrm{ep}})$ to between seven and nine digits was reported; see Table 7.1.
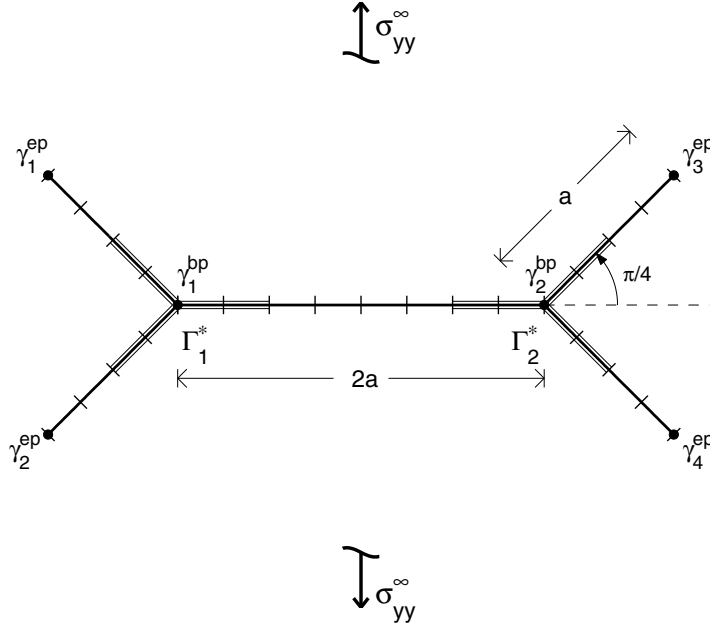
FIG. 7.5. *The "doubly symmetrically branched crack" has $p = 4$ endpoints. The curve segments where the recursion (5.22)–(5.25), (5.30)–(5.33) takes place are denoted $\Gamma_j^{\star bp}$, $l = 1, \ldots, p - 2$.*

The right image of Figure 7.4 shows that the number of GMRES iterations needed to reach a stopping criterion threshold of ϵ_{mach} in the relative residual is rather insensitive to system size. It grows slowly with the number of corners, saturating at about 27.

7.3. Basic branched cracks. The symmetrically branched crack in Figure 2.1 and the doubly symmetrically branched crack in Figure 7.5 may look more complicated than the simple V-shaped crack. But from a numerical viewpoint, once the geometry is implemented into the codes for schemes (I) and (II), they are actually somewhat easier to deal with. The stress field close to branching points γ_j^{bp}, albeit complicated in terms of wedge eigenvalue analysis, is generally less singular and easier to resolve with purely numerical techniques than the stress field close to corner points γ_l^{cp}.

We compute $F(\gamma_2^{\mathrm{ep}})$ for the symmetrically branched crack and $F(\gamma_3^{\mathrm{ep}})$ for the doubly symmetrically branched crack. The geometric constant c in (6.2) is chosen as $c = \mathsf{a}(1 + \cos(\pi/4)/2)$ and as $c = \mathsf{a}(1 + \cos(\pi/4))$ in accordance with [9]. The convergence with mesh refinement for scheme (I) and the convergence with the number of recursion steps for scheme (II) are very similar to that of the V-shaped crack, shown in Figures 1.1 and 7.1, but full convergence in scheme (II) is already reached at $n = 40$ recursion steps. We refrain from showing convergence plots, but collect converged results in Table 7.2.

7.4. The 176-ply branched crack. A more challenging problem for branched cracks was suggested by Englund [9] and is illustrated in Figure 7.6. Normalized stress intensity factors at the endpoints A and C are sought. Englund [12] unintentionally interchanged the positions of the endpoints B and C in Figure 7 of [9], so his results, denoted F_{I}^B and F_{II}^B, actually refer to the endpoint C.

TABLE 7.2
Normalized stress intensity factors $F(\gamma_2^{\mathrm{ep}}) = F_{2\mathrm{I}} + \mathrm{i}F_{2\mathrm{II}}$ for the symmetrically branched crack and $F(\gamma_3^{\mathrm{ep}}) = F_{3\mathrm{I}} + \mathrm{i}F_{3\mathrm{II}}$ for the doubly symmetrically branched crack with $\sigma^\infty = \sigma_{yy}^\infty$.

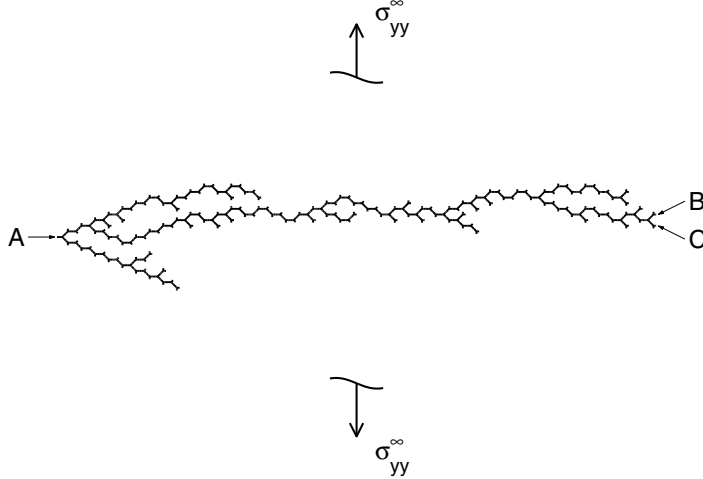| Author	$F_{2\mathrm{I}}$	$F_{2\mathrm{II}}$	$F_{3\mathrm{I}}$	$F_{3\mathrm{II}}$
Present	0.49976895447405	0.47434149296857	0.51963808574113	0.45609973514397
Ref. [9]	0.499768954474	0.474341492965	0.519638086	0.456099735
Ref. [4]	0.536	0.474		
Ref. [29]			0.517	0.455

FIG. 7.6. *The 176-ply branched crack with $p = 178$ endpoints, three of which are A, B, and C.*

Englund's scheme is similar to our scheme (I) but was implemented in Fortran and executed on a SunBlade 100 workstation [9]. It was pushed to the limit of exhaustion for the 176-ply branched crack problem. With about $7 \cdot 10^5$ discretization points on Γ and 350 GMRES iterations, it took about 200 hours to produce the results $F_{\mathrm{I}}^A = 0.615344$, $F_{\mathrm{II}}^A = 0.003233$, $F_{\mathrm{I}}^B = 0.400081$, and $F_{\mathrm{II}}^B = 0.068569$. It is important to keep in mind that this pioneering work was undertaken seven years ago and its main purpose was to show that stable algorithms for these types of problems were at all possible. We are thankful to Dr. Englund for providing us with his routine for the generation of the curve Γ in Figure 7.6.

With 45056 discretization points on Γ and 232 GMRES iterations, our scheme (II) produces the converged results $F_{\mathrm{I}}(\mathsf{A}) = 0.615343681145$, $F_{\mathrm{II}}(\mathsf{A}) = 0.003232637737$, $F_{\mathrm{I}}(\mathsf{C}) = 0.400081251167$, and $F_{\mathrm{II}}(\mathsf{C}) = 0.068568584972$, which confirms the results of Englund [9] and adds another six digits of accuracy. The computing time is about 7 minutes, of which 90% is spent in the GMRES iterative solver. We use $n = 100$ steps in the recursion for the $\mathbf{R}_m$ matrices, which really is not necessary, but also take advantage of the fact that the diagonal blocks of the $\mathbf{R}_m$ matrices are similar. All the $\Gamma_j^{\star\mathrm{bp}}$ have the same shape; only their orientations differ.

8. Discussion. Reduction [25] has been a standard tool for *proving* existence and uniqueness of solutions to singular integral equations on planar curves since the early 1940s. Reduction is not a standard tool for *solving* such equations in scientific computing, even though recent work shows a growing awareness of its numerical potential also in higher dimensions [15]. If one prefers to discretize solely on uniform

meshes, or to use power series solution methods, or does not seek high accuracy and speed, reduction is less important. It may be regarded as unnecessarily complicated.

For large-scale problems, when high accuracy is of interest, and when the curve on which the singular integral equation is to be solved is only piecewise smooth, the need for reduction becomes critical. As for discretization strategies, standard techniques are local mesh refinement and special basis functions. The drawbacks with mesh refinement were discussed in section 1.3. The drawbacks with special basis functions relate to their construction. It involves multiwedge eigenvalue analysis which seems hard to apply, and even harder to automate, for complicated curves. It is difficult to find efficient sets of basis functions when the eigenvalues are closely spaced. The more robust current algorithms for solving reduced singular integral equations on piecewise smooth curves use a mix of the two standard techniques [8].

One can view recursive compressed inverse preconditioning, that is, scheme (II) of this paper, as a competitive alternative to standard discretization. The local mesh refinement is not visible on the coarse grid upon which the integral equation is solved. The manual construction of special basis functions is replaced with an automated procedure which computes an efficient basis for the problem at hand in a purely numerical way. This offers greater flexibility and higher achievable accuracy. Our numerical examples demonstrate convergence to almost optimal accuracy.

A major difficulty when solving reduced singular integral equations is the presence of composed integral operators. The discretization of composed operators leads to matrices whose elements are not cheaply accessible. A locally refined discretization of the individual operators has consequences for all elements in the matrix corresponding to the composed operator. In the present paper we resolve this problem by treating combinations of parts of the individual operators separately. The price for this is four, not one, right inverse preconditioners.

For simplicity, all our numerical examples involved curves made up of straight line segments. But no particular geometric properties of straight lines or wedges are used in the recursion. Curves made up of nonstraight segments can be treated with the same ease. We speculate that our scheme can also be applied to a broader class of integral equations with composed operators on nonsmooth curves, including equations modeling scattering for acoustic waves. See Chapter 3 of [6].

REFERENCES

[1] J. Bremer and V. Rokhlin, *Efficient discretization of Laplace boundary integral equations on polygonal domains*, J. Comput. Phys., 229 (2010), pp. 2507–2525.

[2] Y. Z. Chen, *Stress intensity factors for curved and kinked cracks in plane extension*, Theor. Appl. Fract. Mech., 31 (1999), pp. 223–232.

[3] Y. Z. Chen, *Integral equation methods for multiple crack problems and related topics*, Appl. Mech. Rev., 60 (2007), pp. 172–194.

[4] Y. Z. Chen and N. Hasebe, *New integration scheme for the branch crack problem*, Engrg. Fract. Mech., 52 (1995), pp. 791–801.

[5] Y. Z. Chen, X. Y. Lin, Z. X. Wang, and N. M. A. Nik Long, *Solution of contact problem for an arc crack using hypersingular integral equation*, Int. J. Comput. Methods, 5 (2008), pp. 119–133.

[6] D. C. Colton and R. K. Kress, *Inverse Acoustic and Electromagnetic Scattering Theory*, 2nd ed., Springer, Berlin, 1993.

[7] J. Englund, *Fast accurate and stable algorithm for the stress field around a zig-zag-shaped crack*, Engrg. Fract. Mech., 70 (2003), pp. 355–364.

[8] J. Englund, *Large scale computations for cracks with corners*, in Advances in Boundary Element Techniques, BeTeQ IV, R. Gallego and M. H. Aliabadi, eds., Queen Mary University of London, London, 2003, pp. 71–76.

[9]   J. ENGLUND, *Stable algorithm for the stress field around a multiply branched crack*, Internat.
      J. Numer. Methods Engrg., 63 (2005), pp. 926–946.
[10] J. ENGLUND, *A Nyström scheme with rational quadrature applied to edge crack problems*,
      Comm. Numer. Methods Engrg., 23 (2007), pp. 945–960.
[11] J. ENGLUND, *A higher order scheme for two-dimensional quasi-static crack growth simulations*,
      Comput. Methods Appl. Mech. Engrg., 196 (2007), pp. 2527–2538.
[12] J. ENGLUND, *private communication*, 2010.
[13] L. GREENGARD AND V. ROKHLIN, *A fast algorithm for particle simulations*, J. Comput. Phys.,
      73 (1987), pp. 325–348.
[14] L. GREENGARD, M. C. KROPINSKI, AND A. MAYO, *Integral equation methods for Stokes flow
      and isotropic elasticity in the plane*, J. Comput. Phys., 125 (1996), pp. 403–414.
[15] F. HANG AND S. JIANG, *Generalized Poincaré-Bertrand formula on a hypersurface*, Appl. Com-
      put. Harmon. Anal., 27 (2009), pp. 100–116.
[16] P. HANSSON AND S. MELIN, *Simulation of simplified zigzag crack paths emerging during fatigue
      crack growth*, Engrg. Fract. Mech., 75 (2008), pp. 1400–1411.
[17] J. HELSING, *On the numerical evaluation of stress intensity factors for an interface crack of a
      general shape*, Internat. J. Numer. Methods Engrg., 44 (1999), pp. 729–741.
[18] J. HELSING AND A. JONSSON, *Stress calculations on multiply connected domains*, J. Comput.
      Phys., 176 (2002), pp. 456–482.
[19] J. HELSING AND R. OJALA, *On the evaluation of layer potentials close to their sources*, J. Com-
      put. Phys., 227 (2008), pp. 2899–2921.
[20] J. HELSING AND R. OJALA, *Corner singularities for elliptic problems: Integral equations, graded
      meshes, quadrature, and compressed inverse preconditioning*, J. Comput. Phys., 227 (2008),
      pp. 8820–8840.
[21] J. HELSING AND G. PETERS, *An efficient numerical algorithm for cracks partly in frictionless
      contact*, SIAM J. Appl. Math., 61 (2000), pp. 551–566.
[22] V. I. KUSHCH, I. SEVASTIANOV, AND L. MISHNAEVSKY, *Effect of crack orientation statistics on
      effective stiffness of microcracked solid*, Internat. J. Solids Structures, 46 (2009), pp. 1574–
      1588.
[23] S. G. MIKHLIN, *Integral Equations and Their Applications to Certain Problems in Mechanics,
      Mathematical Physics and Technology*, 2nd ed., Pergamon Press, London, 1964.
[24] S. G. MIKHLIN, N. F. MOROZOV, AND M. V. PAUKSHTO, *The Integral Equations of the Theory
      of Elasticity*, Teubner, Leipzig, Germany, 1995.
[25] N. I. MUSKHELISHVILI, *Singular Integral Equations*, 2nd ed., P. Noordhoff N.V., Groningen,
      The Netherlands, 1953.
[26] A. V. PHAN AND S. MUKHERJEE, *Boundary contour method fracture analysis of bimaterial
      interface cracks*, Comm. Numer. Methods Engrg., 24 (2008), pp. 1685–1697.
[27] T. RABCZUK AND G. ZI, *A meshfree method based on the local partition of unity for cohesive
      cracks*, Comput. Mech., 39 (2007), pp. 743–760.
[28] Y. SAAD AND M. H. SCHULTZ, *GMRES: A generalized minimal residual algorithm for solving
      nonsymmetric linear systems*, SIAM J. Sci. Stat. Comput., 7 (1986), pp. 856–869.
[29] V. VITEK, *Plane strain stress intensity factors for branched cracks*, Internat. J. Fracture,
      13 (1977), pp. 481–501.
[30] A. K. YAVUZ, S. L. PHOENIX, AND S. C. TERMAATH, *An accurate and fast analysis for strongly
      interacting multiple crack configurations including kinked (V) and branched (Y) cracks*,
      Internat. J. Solids Structures, 43 (2006), pp. 6727–6750.